J Electr Eng Technol.2018; 13(4): 1614-1622
http://doi.org/10.5370/JEET.2018.13.4.1614

ISSN(Print) 1975-0102
ISSN(Online) 2093-7423

# Detection and Classification of Demagnetization and Short-Circuited Turns in Permanent Magnet Synchronous Motors

**Young-Woo Youn*, Don-Ha Hwang*, Sung-ju Song** and Yong-Hwa Kim†**

**Abstract** – The research related to fault diagnosis in permanent magnet synchronous motors (PMSMs) has attracted considerable attention in recent years because various faults such as permanent magnet demagnetization and short-circuited turns can occur and result in unexpected failure of motor related system. Several conventional current and back electromotive force (BEMF) analysis techniques were proposed to detect certain faults in PMSMs; however, they generally deal with a single fault only. On the contrary, cases of multiple faults are common in PMSMs. We propose a fault diagnosis method for PMSMs with single and multiple combined faults. Our method uses three phase BEMF voltages based on the fast Fourier transform (FFT), support vector machine(SVM), and visualization tools for identifying fault types and severities in PMSMs. Principal component analysis (PCA) and t-distributed stochastic neighbor embedding (t-SNE) are used to visualize the high-dimensional data into two-dimensional space. Experimental results show good visualization performance and high classification accuracy to identify fault types and severities for single and multiple faults in PMSMs.

**Keywords**: Permanent magnet synchronous motor, Fault diagnosis, Signal processing.

## 1. Introduction

Permanent magnet synchronous motors (PMSMs) are widely used in electric vehicles, renewable energy generation, and many other industries as major electrical machines because of their high-speed operation and precise torque control [1]. Various types of electrical motor faults may occur even though the motor is continuously monitored [2]. Faults in PMSMs may lead to degraded motor efficiency and related system performance, thereby causing catastrophic accidents. Therefore, it is important to monitor or diagnose the state of PMSMs. The rotor and stator those are most important components of the PMSM decide the performance and reliability of the entire motor related system. Permanent magnet (PM) demagnetization and short-circuited turns are common critical faults in the rotor and stator of PMSMs, respectively. These faults arise essentially due to manufacturing defects as well as electrical, mechanical, thermal, and other environmental influences [3]. Therefore, detection and classification of PM demagnetization, short-circuited turns, and related multiple faults are crucial for reliable operation of PMSMs.

The irreversible demagnetization of the rotor is a serious problem that reduces the output torque of the PMSMs and degrades the motor characteristics [4]. The major cause of this fault is its operating phenomenon. During normal operation of the PMSMs, the electrical current produces inverse magnetic field that opposes the permanent magnets' remainder induction. The PMs become demagnetized over a part of the pole (partial demagnetization) or all over the pole (uniform demagnetization) due to this repetitive operating state [3]. High temperature may also cause the demagnetization of the permanent magnet. The short-circuited turns, which results in stator winding insulation degradation can also occur during operation and is recognized as a critical fault in PMSMs. A combination of thermal, environmental, and electrical strains such as high switching frequency, voltage spikes caused by impedance mismatch, etc. cause the short-circuited turns [3]. When short-circuited turns occur in the stator winding, the symmetry of the motor is damaged, leading to a reverse rotating field, which decreases the output torque of the PMSMs and increases the current loss. Furthermore, it may partially demagnetize the permanent magnet of the rotor. Therefore, these two types of faults may occur independently or simultaneously.

Many studies have been reported over the years to diagnose PM demagnetization and short-circuited turns. For detecting PM demagnetization, conventional methods of using a magnetic viewer or gauss meter to measure the magnets' quality are applied due to their high accuracy. These methods, however, are executed in stopped and disassembled motor conditions. PM demagnetization detection via related frequency is also proposed using stator current analysis [5, 6]. In [7, 8], back electromotive force (BEMF) analysis is also proposed to detect PM demagnetization. These methods only use the magnitude and signature of BEMF due to their processing in the time

† Corresponding Author: Dept. of Electronic Engineering, Myongji University, Korea. (yongkim@mju.ac.kr)
* HVDC Research Division, Korea Electrotechnology Research Institute (KERI), Korea. ({ywyoun, dhhwang}@keri.re.kr)
** Dept. of Electronic Engineering, Myongji University, Korea. (chess12@naver.commailto, gilsoon@kiee.or.kr)
Received: March 9, 2017; Accepted: March 19, 2018

domain. To increase the accuracy of fault detection, BEMF signature and its harmonic characteristics analysis is also suggested [9]. However, these methods only consider not multiple combined faults those can be occurred with demagnetization of rotor but single fault.

To detect short-circuited turns, BEMF and stator current analysis methods have been used in the industry. In [10], BEMF estimator is proposed to identify short-circuited turns. It uses average difference between the estimated and reference BEMF as a fault index. However, its disadvantage is that the reference BEMF is difficult to calculate when the detailed motor specifications are not given. In [11], magnitude of the stator current is suggested for the fault detection as the current through the faulted coils increases. Although signal analysis of short-circuited turns has been inspected, no fault index (or indicator) and classifier has been suggested for identification and classification. Harmonics of the phase current spectrum are exploited as fault indices using the 5th and 7th harmonics [12] and using only the 9th harmonic [13]. Ebrahimi and Faiz proposed a stator current frequency pattern using fractional harmonics and competent criterion to detect and classify the occurrence and number of shorted turns using a support vector machine (SVM) as a classifier [14]. Using the 3rd, 5th, 7th, and 9th harmonics of the phase current spectrum, short-circuited turns were detected depending on the winding configuration of the motor [15]. Using the 3rd harmonic amplitude of the stator phase current signals as the fault index, an artificial neural network (ANN) based scheme was proposed to detect short-circuited turns and their severities [16]. However, this applies to short-circuited turns but not PM demagnetization, which is also a major fault and has a similar frequency pattern to the stator current of PMSMs.

This paper considers single and multiple combined faults in PMSMs such as PM demagnetization, short-circuited turns, and multiple combined faults with both PM demagnetization and short-circuited turns. We present a diagnosis method for fault type and their severity detection based on the fast Fourier transform (FFT), SVM, and dimensionality reduction tools. The fault detection method focuses on the spectrum of BEMF voltage signals and uses the amplitudes of fault-related frequency harmonics in three phases as fault indices. There are online and offline based methods for measuring the BEMF voltage signals of the PMSMs. In the online environment where a test motor acts as a role of motor, the signals should be measured in real time under different load conditions. In the offline environment, a simple method to measure the signals is based on the condition that the test motor operates as a generator. This paper focuses on the offline environment and the BEMF signals are measured at no load condition of a test motor. The multi-class SVM is used for the classification of different fault types and severities in motors [17-20]. For dimensionality reduction tools, principal component analysis (PCA) and t-distributed stochastic neighbor embedding (t-SNE) are considered, where PCA is a common statistical technique based on data variance preservation for feature extraction and dimensionality reduction [21, 22] and t-SNE is another dimensionality reduction technique based on topological preservation for visualizing high-dimensional data [23]. When reducing the dimensionality of data, PCA is the linear technique with focus on keeping the low-dimensional representations of dissimilar data points far apart and t-SNE is the non-linear technique to maintain the structure of different classes without class labels. In this paper, PCA and t-SNE reduced the dimensionality of fault indices down to 2. The proposed diagnostic method can discriminate between different fault types and severities under different velocity conditions. The following highlights our contributions:

- For fault type and their severity detection in PMSMs, the proposed approach analyses the harmonics of the spectrum of BEMF voltage under PM demagnetization, short-circuited turns and multiple combined faults with both PM demagnetization and short-circuited turns.
- Experimental results show that the fault indices obtained from three phases show better classification performance than the fault indices from the single phase.
- PCA and t-SNE are used to reduce the dimensionality of fault indices. Experimental results show that the first 2 Principal Components from the PCA are effective for classification. t-SNE enables the visual inspection of important structural characteristics for fault types and severities in PMSMs.

## 2. Experimental Set-Up and Faults in PMSMs

### 2.1 Experimental Set-Up

Experimental tests were performed using PMSM (NdFe35 magnet). The specifications of the PMSM are summarized in Table 1. The PMSM test system, which consists of a test motor, load motor, data acquisition system (Data), and an inverter is represented in Fig. 1. The inverter is connected to the load motor for BEMF generation of the test motor.

To measure the BEMF, the inverter connected to the load motor controls the test motor rotated at 300 and 500 r/min. The DAS was set by a sampling frequency of 50 kHz and acquisition time of 5.24288 s for the discrete-time signal

**Table 1.** Characteristics of the test motor used in experiments

| Item | Value |
|---|---|
| rated power | 42.7 kW |
| maximum power | 81.4 kW |
| maximum speed | 9800 rpm |
| number of poles | 8 |
| number of slot | 48 |
| number of series turns in a phase | 20 |
| number of parallel circuit in a phase | 4 |

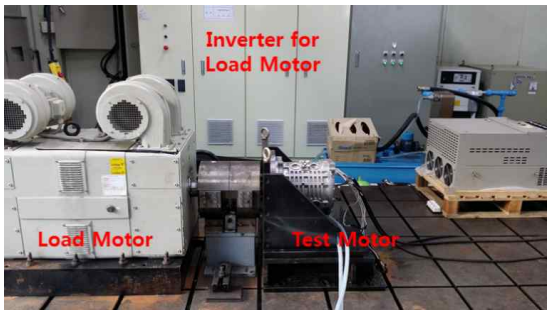


**Fig. 1.** Experimental set-up

**Table 2.** Average residual magnetic flux density of rotors

| Motor condition | Average magnetic flux density (T) |
|---|---|
| Normal | 2.8 |
| Demagnetized rotor | 1.19 |

$x_s[n]$, where $n = 1, 2, \cdots, N_s$ and $N_s = 2^{18}$

### 2.2 Faults in PMSMs

Four different types of PMSM conditions were diagnosed: a healthy motor, motor with demagnetization, motor with short-circuited turns, motor with multiple combined faults (demagnetization and short-circuited turns).

To simulate the demagnetized motor, a disassembled rotor was put into the dry oven for high temperature influence on the rotor magnet. The demagnetized rotor was 42% demagnetized compared to the normal condition of the rotor. Table 2 represents the average residual magnetic flux density of rotors calculated using a magnetic viewer. BEMF signature analysis and frequency component of stator current can be used for detecting PM demagnetization [5-9]. PM demagnetization related frequency component of the stator current is given by

$$f_{PMdemag} = f_s\left(1 \pm \frac{n}{p}\right) \tag{1}$$

where $f_s$ is the fundamental frequency, $n$ is an integer, and $p$ is the number of pole pairs.

Fig. 2 shows the design of short-circuited turns of the motor. The motor has distributed windings with four parallel 20 turn windings per phase. Each parallel circuit consists of two series 10 turn windings. The motor was reconfigured to have access to 1, 3, and 5 of 20 series turns in a parallel circuit of phase 'a' to simulated the fault.

Similar to the PM demagnetization detection, BEMF and stator current signal analysis have been used for identifying the short-circuited turns in motors. When the short-circuited turns occur, the frequency components of stator current appear and are represented as

$$f_{short-circuited\ turns} = f_s\left(1 \pm \frac{2K_{sa}+1}{p}\right) \tag{2}$$

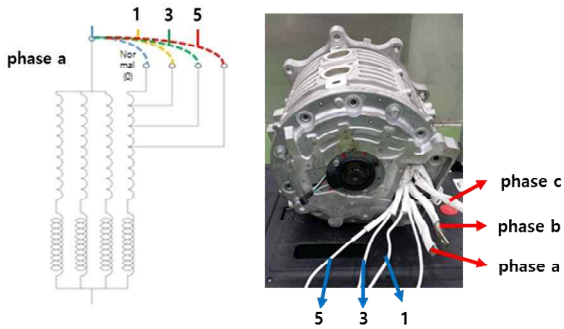


**Fig. 2.** Test motor with short-circuited turns

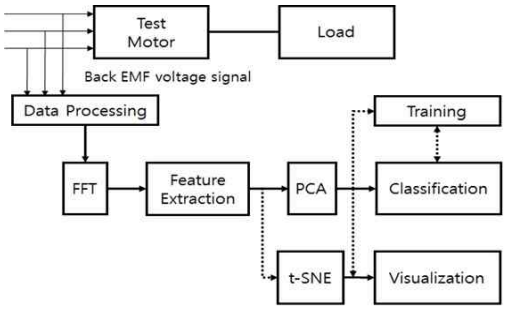


**Fig. 3.** Block diagram of the proposed fault diagnosis system

where $K_{sa}$ is the constant coefficient.

The common cause of the short-circuited turns and demagnetization is thermal stress. In addition, short-circuited turn faults generate high temperature to the motor and this can lead to the PM demagnetization. Therefore, these two types of faults may occur together. To analyze the phenomenon of the multiple combined fault motors (demagnetization and short-circuited turns), in this paper, the motor was designed by assembling the demagnetized rotor into the stator that has short-circuited turns.

## 3. Proposed Fault Detection and Classification

The block diagram of the proposed fault detection and classification is illustrated in Fig. 3, where the proposed scheme consists of frequency domain analysis, feature extraction, classification, and visualization.

### 3.1 Feature extraction

The BEMF voltage signals in phases a, b, c are processed by FFT, and peak values of the defect frequency and harmonics in the $i$ th measurement, $P_k^x(i)$, are obtained by the amplitude of the maximum peak located in the frequency band that is centered at the $k$ th defect frequency harmonic, $f_k^x$ with a bandwidth BW. Here, $k$ is the number of harmonics in the spectrum and $x$ represents phases $a$, $b$, and $c$. The normalized peak values of the $i$ th measurement are defined by

$$A_k^x(i) = \frac{P_{k+1}^x(i)}{P_1^x(i)} \tag{3}$$

where $k = 1, 2, \cdots, K-1$, $i = 1, 2, \cdots, M$, and $x = a, b, c$.

Transformation of the time-domain BEMF voltage signal to frequency domain via Fourier transform reduced the dimension of each signal from $N_c$ to $N_c/2$. Feature extraction in (3) generated fault diagnostic indices with $3(k-1)$ frequency-domain BEMF signals and $3(N_c/2)$ feature dimension in phases *a*, *b*, and *c*. PCA further reduced the dimensionality for classification and visualization.

### 3.2 Principal component analysis

PCA is a statistical technique for the reduction of the high-dimensional data into low-dimensional data. The feature data vector $\mathrm{a}_i$ from (3) can be defined by

$$\begin{aligned}\mathrm{a}_i = \Big[ & A_1^a(i), \cdots, A_{K-1}^a(i), A_1^b(i), \cdots, \\ & A_{K-1}^b(i), A_1^c(i), \cdots, A_{K-1}^c(i) \Big]^T\end{aligned} \tag{4}$$

The covariance matrix can be obtained by

$$\Sigma = \frac{1}{N}\sum_{i=1}^{N}(\mathrm{a}_i - \boldsymbol{\mu})(\mathrm{a}_i - \boldsymbol{\mu})^T \tag{5}$$

where the mean vector $\boldsymbol{\mu}$ is calculated as $\boldsymbol{\mu} = (1/N)\sum_{i=1}^{N}\mathrm{a}_i$.

By using eigenvalue decomposition, the eigenvalues And Corresponding Eigenvectors of $\sum$ Are Represented By $\{\lambda_1 \ge \lambda_2 \ge \cdots \ge \lambda_{3(K-1)}\}$ and $\{u_1 \ge u_2 \ge \cdots \ge u_{3(K-1)}\}$, respectively. By taking into account the number of principal components *d*, we can define a transformation matrix $\boldsymbol{U} = [u_1 u_2 \cdots u_d]^T$ associated with the largest *d* eigenvalues. Then, the principal component vector $\mathrm{s}_i$ in the *i* th measurement can be obtained by

$$\mathrm{s}_i = \boldsymbol{U}(\mathrm{a}_i - \boldsymbol{\mu}) \tag{6}$$

The principal component vector $\mathrm{s}_i$ is considered as the fault diagnostic vector to classify fault motors. For the purpose of the dimensionality reduction and data visualization, only the eigenvectors corresponding to the two largest eigenvalues are selected and the input feature vectors are projected on them to get a *d*=2 dimensional representation.

### 3.3 Classification

The classification of the proposed scheme is based on linear multi-class SVM classification to detect fault types and their severities. The basic idea of the SVM was thoroughly developed based on the statistical learning theory [17, 18]. The basic SVM deals with two-class problems i.e. separating two classes by a hyperplane that is defined by a number of support vectors. To classify multiple classes, two techniques are implemented: "one-against-one" and "one-against-all" [24]. One-against-one technique classifies the classes in pairs and then uses a binary SVM to differentiate each pair of classes. For a problem with $m$ classes, $m(m-1)/2$ SVMs are trained to identify one class from another class and then one class is selected using maximum voting, where *m* is the number of classes and each SVM votes for one class. One-against-all technique is based on the creation of m number of SVM binary classifications to separate one class from the others. Then, the classification is achieved using the maximum output from the results of all SVMs. For multi-class SVMs, one-against-one technique will be used, as the training time is shorter [24].

The SVM is trained using the $\upsilon$-fold cross-validation to optimize the parameter $C$ for the multi-class linear SVM, where $C > 0$ is the penalty parameter of the error term and $\upsilon = 5$. With the optimal $C$ value, the entire training data set is used to define a hyperplane for the linear SVM. Then, the test set is classified to detect the motor fault and its severity.

### 3.4 Visualization

t-SNE is another dimensionality reduction technique that was recently developed for data visualization and aims to convert high-dimensional data to the low-dimensional space while retaining their pair-wise similarities [23]. High-dimensional data $\mathrm{a}_i$ are projected to the low-dimensional vector $\mathrm{b}_i$ in the projection, where $i = 1, \cdots, N$ and $\mathrm{b}_i = [b_1(i) \cdots b_d(i)]^T$. In the t-SNE, a Kullback-Leibler (KL) divergence between the joint probability distributions of the low-dimensional embedding and the high-dimensional data is defined as

$$KL(P \| Q) = \sum_{i \ne j} p_{ij} \log \frac{p_{ij}}{q_{ij}} \tag{7}$$

where $P$ and $Q$ are in high-dimensional and low-dimensional space, respectively. In (7), $p_{ij}$ represents the pairwise similarities for the pair $(\mathrm{a}_i, \mathrm{a}_j)$ in the high-dimensional space and is defined as

$$p_{ij} = \frac{\exp\left(-\dfrac{\|\mathrm{a}_i - \mathrm{a}_j\|^2}{2\sigma^2}\right)}{\sum_k \sum_{l, l \ne k} \exp\left(-\dfrac{\|\mathrm{a}_k - \mathrm{a}_l\|^2}{2\sigma^2}\right)} \tag{8}$$

where $\sigma^2$ is the variance of the distribution $p_{ij}$. In the

low-dimensional space, $q_{ij}$ uses a Student's-t distribution to compute the similarity between the two points and is defined as

$$q_{ij} = \frac{\left(1+\left\|\mathrm{b}_i - \mathrm{b}_j\right\|^2\right)^{-1}}{\sum_k \sum_{l,l\neq k}\left(1+\left\|\mathrm{b}_k - \mathrm{b}_l\right\|^2\right)^{-1}} \quad (9)$$

By minimizing the KL divergence in (7), t-SNE reduces the dimensionality of the original data and retains their pairwise similarities.

For the visualization of relevance of PMSM faults, t-SNE reduces the dimensionality from $3(k-1)$ dimension to 2 dimensional spaces.

## 4. Experimental Results

To validate the feasibility of the proposed method, experimental set-up and faults in PMSMs have been shown in Section 2. The conditions of faulty PMSMs are described in Table 3. Using experimental results, the effects of demagnetization, stator inter-turn, and multiple combined faults are analyzed in this Section.

Fig. 4 shows the normalized BEMF voltage spectrum for the healthy and faulty PMSMs when operating at 300 rpm. When stator inter-turn faults occur in PMSMs, the stator currents spectrum may contain odd harmonics of electrical frequency [12, 13, 15]. As shown in Fig. 4, the BEMF voltage spectrum contains the third, fifth, and ninth harmonics of the electrical frequency in the spectrum for the healthy and faulty motors. It is observed that the third harmonic amplitude for faulty motors is lower than that for healthy motors. In addition, the seventh harmonic of the electrical frequency appears in case of demagnetization faults (demagnetization faults and multiple combined faults with demagnetization and turn-short). However, the fractional harmonics predicted by (1) and (2) are not present in the BEMF voltage spectrum. From the voltage spectrum, the healthy motors are distinguished from faulty motors using the third harmonic, but it is not possible to find any fault index for diagnosing fault types.

Fig. 5 shows the cumulative distributive functions (CDFs) of the variations of BEMF voltage amplitudes of

**Table 3.** Description of faulty PMSMs

| Class Number (Representation) | Fault conditions |
|---|---|
| 1 (Healthy) | Healthy motors |
| 2 (Turn#1) | 1 short-circuited turn |
| 3 (Turn#3) | 3 short-circuited turns |
| 4 (Turn#5) | 5 short-circuited turns |
| 5 (DM) | Demagnetization |
| 6 (DM&Turn#1) | Combined faults with demagnetization and 1 short-circuited turn |
| 7 (DM&Turn#3) | Combined faults with demagnetization and 3 short-circuited turns |
| 8 (DM&Turn#5) | Combined faults with demagnetization and 5 short-circuited turns |

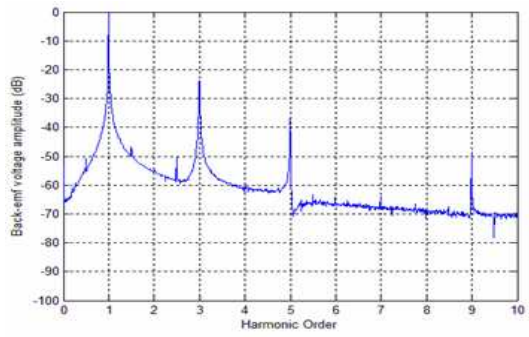


(a) Healthy motor

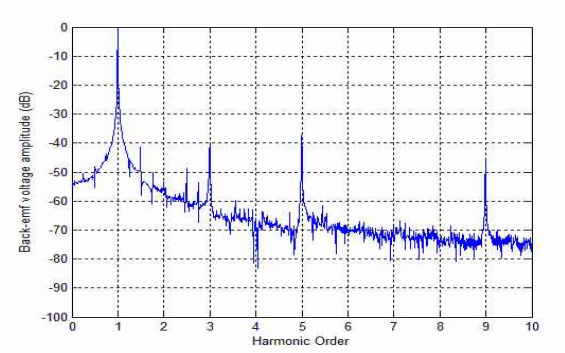


(b) Motor with 1 short-circuited turn

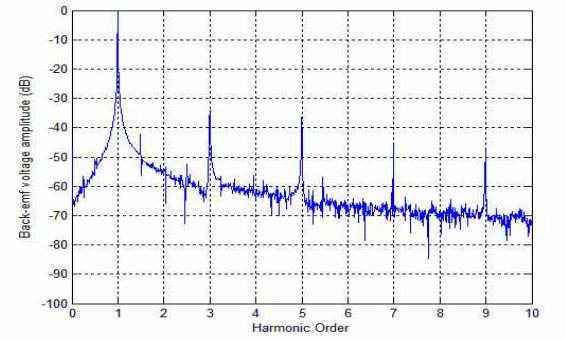


(c) Motor with demagnetization

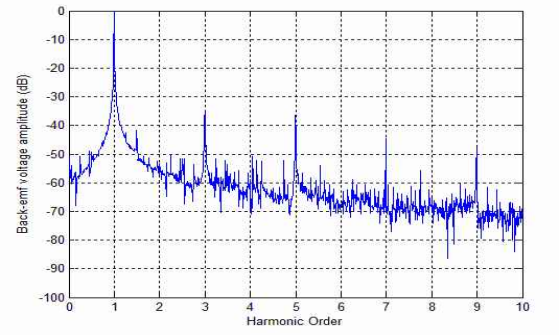


(d) Motor with multiple combined faults with demagnetization and 1 short-circuited turn

**Fig. 4.** BEMF voltage spectrum of PMSMs operating at 300 rpm

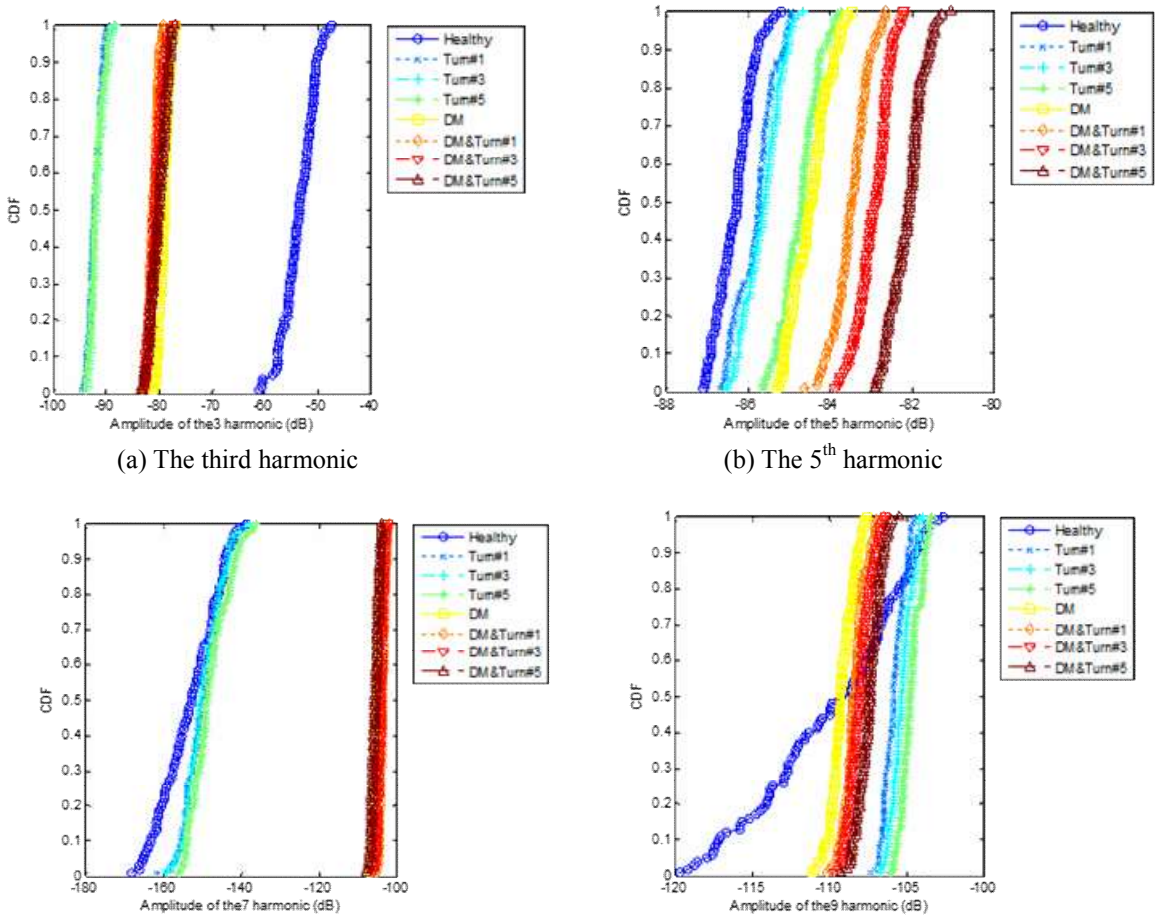


(a) The third harmonic

(b) The 5th harmonic

(c) The 7th harmonic

(d) The 9th harmonic

**Fig. 5.** CDFs of amplitudes of fault harmonics operating at 300 rpm

harmonics in phase $a$ when operating at 300 rpm. We see that the third harmonic amplitude for the healthy motor is larger than that of the faulty motor [15, 16]. As expected, the spectrum around the seventh harmonic is clear enough to detect a group of healthy and stator inter-turn short motor faults from a group of demagnetization and multiple combined faults [12, 15]. However, there is no specific harmonic amplitude to classify all types of faults separately. In this paper, the amplitudes of harmonics in phases *a*, *b*, and *c* are used as fault diagnostic indices.

The SVM-based classification results with fault diagnostic indices are summarized in Table 4. In the training processes, to optimize the parameter $C$ for the linear SVM, we use five-fold cross-validation to test all values of $C = \left\{2^{-15}, 2^{-14.9}, \cdots, 2^{15}\right\}$. Using the training set, five-fold cross-validation accuracies are obtained by the grid search, where the cross-validation accuracy is the percentage of data that are correctly classified. The values corresponding to the best cross-validation accuracies are then selected. With the optimal parameters, the entire training data set was trained again to define hyperplane for multi-class SVM classifiers. It is observed that the diagnostic performance with 12 harmonics from three phases improves compared with those with four harmonics from a single phase. In the case of 300 and 500 rpm, the accuracy results are increased by 19.58% and 6.25%, respectively, compared to the results using four harmonics from single-phase a. Maximum values of the classification using 12 harmonics in three phases reach 99.58% and 99.17% for 300 and 500 rpms, respectively. Furthermore, PCA can reduce the dimensionality from 12 to 2 for visualization and classification.

**Table 4.** Classification results using harmonics by multi-class SVM

| Speed (rpm) | Phase | Feature types (harmonics) | Accuracy (%) | C Value |
|---|---|---|---|---|
| 300 | a,b,c | 12 | 99.5833 | 1024 |
| 300 | a | 4 | 80 | 1176.3 |
| 300 | b | 4 | 77.75 | 13512 |
| 300 | c | 4 | 90.8 | 222.8609 |
| 500 | a,b,c | 12 | 99.1667 | 3.0518e-5 |
| 500 | a | 4 | 92.91 | 64 |
| 500 | b | 4 | 85 | 1351.1761 |
| 500 | c | 4 | 96.67 | 39.3966 |

Fig. 6 shows the first two principal components (PCs) using 12 harmonics from three phases operating at 500 rpm. The selected PCs are given by the linear combination of 12

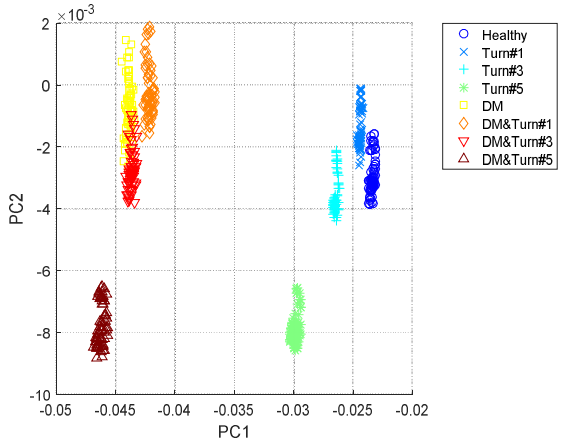


**Fig. 6.** Feature extraction using PCA

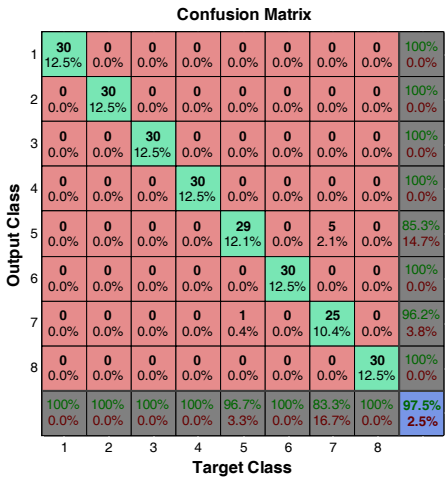


**Fig. 7.** Confusion matrix using PCA by multi-class SVM

harmonics and the 3rd harmonic components in phases *a*, *b*, and *c* are the most significant components to from the considered PCs. It can be observed that three fault types for healthy, stator inter-turn, and PM demagnetization and combined multiples faults are well separated. Nevertheless, the separation for demagnetization and multiple combined faults is not adequate and in fault severity cases, they overlap.

Fig. 7 shows the confusion matrix obtained from the proposed algorithm with PCA-based two principal components operating at 300 rpm, where the true class labels are along the x-axis and the class predictions of the proposed algorithm are along the y-axis. The diagonal are the correct classifications, whereas all the other entries show misclassifications. The bottom right cell shows the overall accuracy of 97.5%. It can be seen that one sample for class 1 (demagnetization) is wrongly predicted as class 7 (combined faults with demagnetization and 3 short-circuited turns) and five samples for the class 7 are wrongly predicted as class 5. The detailed PCA-based classification results of each condition are shown in Table 5. It is evident that the proposed approach delivers

**Table 5.** Classification results using PCA by multi-class SVM

| Speed (rpm) | Accuracy (%) | C Value |
|---|---|---|
| 300 | 92.5 | 3565 |
| 500 | 97.5 | 2702.3522 |

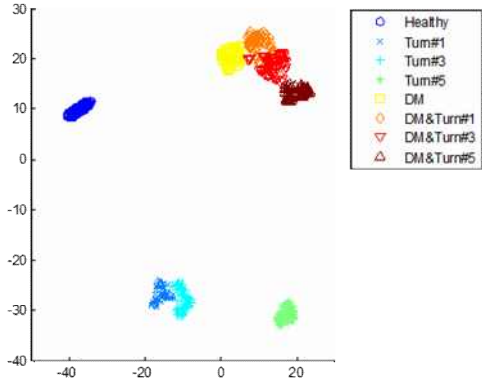


**Fig. 8.** t-SNE representation of the feature vectors of the 12 harmonics in the training data set

superior diagnostic performance using two principal components from three phases compared to the case using four harmonics from single phase.

Fig. 8 shows how t-SNE groups all training samples operating at 500 rpm on the 2D representation, where t-SNE reduces the dimensionality from 12 to 2 for classification. This technique makes it possible to embed these 12 dimensional vectors in a two-dimensional plot in such a way that the vectors that are close together in the 12 dimensional spaces are also close together in the two-dimensional plot. Classes such as healthy motor, stator inter-turn faulty motors, and demagnetization faulty motors are clearly separated from the other classes. Multiple combined faults are difficult to classify from demagnetization faults, one short circuited-turn is close to three short circuited turns and 5 short circuited-turns is a different cluster from one short circuited turn and three short circuited turns, which support the feature extraction results using PCA as shown in Fig. 6. For visualization, there is a significant improvement over the PCA visualization results in Fig. 6. In contrast to PCA, t-SNE has a non-convex objective function and the objective function is minimized using a gradient descent optimization with random initialization, so different runs can generate different results. Therefore, t-SNE has been used for the visualization analysis of fault characteristics.

## 5. Conclusion

PM demagnetization, stator inter-turn, and multiple combined faults with stator inter-turn fault and PM demagnetization may severely deteriorate PMSM

performance. In this paper, based on harmonic analysis of BEMF voltage spectrum, we have proposed the fault diagnosis method based on the FFT, SVM, and dimensionality reduction tools (PCA and t-SNE) for detecting and classifying various types and severities of faults in PMSMs. The analysis of the experimental results showed that the diagnostic performance with 12 harmonics from BEMF voltages of three phases was higher than that with four harmonics from BEMF voltages of single phase. The proposed PCA-based method efficiently provides more accurate classification results of different fault types and severities in PMSMs, compared to four harmonics in a single phase. In PCA, the 3rd harmonic components in the phases *a*, *b*, and *c* are the most significant components to from the considered principle components. In addition, t-SNE exhibits better visualization performance over PCA for discriminating between different fault types and severities in PMSMs. The proposed visualization approach will be useful to analyze features from other motor-related faults detections such as eccentricity fault and bearing faults. In future, the proposed method will be investigated in partial demagnetization of PMSMs by performing further analysis and experiments. For a robust detection of fault type and their severity in PMSMs, several experiments for partial demagnetization and more short circuited turns should be included in the experimental setup.

## Acknowledgements

This work was supported in part by Korea Electrotechnology Research Institute (KERI) Primary research program through the National Research Council of Science & Technology (NST) funded by the Ministry of Science, ICT and Future Planning (MSIP) (No. 16-12-N0103-09), in part by the 2016 Research Fund of Myongji University, and in part by Basic Science Research Program through the National Research Foundation of Korea (NRF) funded by the Ministry of Science, ICT & Future Planning (NRF-2017R1C1B1012259).

## References

[1] Jongman Hong, Sanguk Park, Doosoo Hyun, Taejung Kang, Sang Bin Lee, Christian Kral, and Anton Haumer, "Detection and Classification of Rotor Demagnetization and Eccentricity Faults for PM Synchronous Motors," *IEEE Trans. Ind. Appl*., vol. 48, no. 3, pp. 923-932, May/June. 2012.

[2] Bilal Akin, Salih Baris Ozturk, Hamid A. Toliyat, and Mark Rayner, "DSP-Based Sensorless Electric Motor Fault Diagnosis Tools for Electric and Hybrid Electric Vehicle Powertrain Applications," *IEEE Trans. Veh. Technol*., vol. 58, no. 5, pp. 2150-2159, June. 2009.

[3] Hamid A. Toliyat, Subhasis Nandi, Seungdeong Choi, and Homayoun Meshgin-Kelk, *Electric machines: modeling, condition monitoring, and fault diagnosis.* CRC Press, 2012.

[4] Ki-Chan Kim, Seung-Bin Lim, Dae-Hyun Koo, and Ju Lee, "The Shape Design of Permanent Magnet for Permanent Magnet Synchronous Motor Considering Partial Demagnetization," *IEEE Trans. Magn.,* vol. 42, no. 10. pp. 3485-3487, Oct. 2006.

[5] Satish Rajagopalan, Wiehan le Roux, Thomas G. Habetler, and Ronald G. Harley, "Dynamic eccentricity and demagnetized rotor magnet detection in trapezoidal flux (brushless DC) motors operating under different load conditions," *IEEE Trans. Power Elect.,* vol. 22, no. 5, pp. 2061-2069, Sep. 2007.

[6] Antonio Garcia Espinosa, Javier A. Rosero, Jordi Cusido, Luis Romeral, and Juan Antonio Ortega, "Fault detection by means of Hilbert-Huang transform of the stator current in a PMSM with demagnetization," *IEEE Trans. Energy Convers.,* vol. 25, no. 2, pp. 312–318, June. 2010.

[7] Yao Da, Xiaodong Shi, and Mahesh Krishnamurthy, "A New Approach to Fault Diagnostics for Permanent Magnet Synchronous Machines Using Electromagnetic Signature Analysis," *IEEE Trans. Power Electron.*, vol. 28, no. 8, pp. 4104-4112, Aug. 2013.

[8] Julio-Cesar Urresty, Jordi-Roger Riba, and Luis Romeral, "A Back-emf Based Method to Detect Magnet Failures in PMSMs," *IEEE Trans, Magn.*, vol. 49, no. 1, pp. 591-598, Jan. 2013.

[9] Hyung-Kyu Kim, Dong-Hyeok Kang, and Jin Hur, "Fault Detection of Irreversible Demagnetization Based on Space Harmonics According to Equivalent Magnetizing Distribution," *IEEE Trans. Magn.,* vol. 51, no. 11, pp. 8109304, Nov. 2015.

[10] Ali Sarikhani, and Osama A. Mohammed, "Inter-Turn Fault Detection in PM Synchronous Machines by Physics-Based Electromotive Force Estimation," *IEEE Trans. Ind. Electron.,* vol. 60, no. 8, pp. 3472-3484, Aug. 2013.

[11] Min Dai, Ali Keyhani, and Tomy Sebastian, "Fault Analysis of a PM Brushless DC Motor Using Finite Element Method," *IEEE Trans. Energy Convers*., vol. 29, no. 1, pp. 1-6, Mar. 2005.

[12] Julio-Cesar Urresty, Jordi-Roger Riba, and Luis Romeral, "Application of the zero-sequence voltage component to detect stator winding inter-turn faults in PMSMs," *Electric Power Systems Research,* vol. 89, pp. 38-44, Aug. 2012.

[13] J. Rosero, and J. Romeral, "Simulation and Fault Detection in PMSM under Dynamic Conditions," *Cedrat Flux Solutions & Mechatronic Products,* 2009.

[14] Bashir Mahdi Ebrahimi, and Jawad Faiz, "Feature Extraction for Short-Circuit Fault Detection in

Permanent-Magnet Synchronous Motors Using Stator-Current Monitoring," *IEEE Trans. Power Electron.,* vol. 25, no. 10, pp. 2673-2682, Oct. 2010.
[15] Harold Saavedra, Julio-Cesar Urresty, and Jordi-Roger Riba, "Detection of inter-turn faults in PMSMs with different winding configurations," *Energy conversion and management,* vol. 79, pp. 534-542, Mar. 2014.
[16] Ferhat Cira, Muslum Arkan, and Bilal Gumus "Detection of stator winding inter-turn short circuit faults in permanent magnet synchronous motors and automatic classification of fault severity via a pattern recognition system," *J Electr Eng Technol,* vol. 11, no. 2, pp. 416-424, Feb. 2016.
[17] Vladimir Vapnik, *The Nature of Statistical Learning Theory.* New York:Springer, 1999.
[18] Christopher J.C. Burges, "A Tutorial on Support Vector Machines for Pattern Recognition," *Data mining and Knowledge Discovery,* vol. 2, no. 2, pp. 121-167, June. 1998.
[19] Bernhard Scholkopf, and Alexander J. Smola, *Learning with Kernels: Support Vector Machines, Regularization, Optimization, and Beyond* The MIT Press, 2002
[20] *A Practical Guide to Support Vector Classification* http://www.csie.ntu.edu.tw/~cjlin/libsvm, accessed 19 Oct. 2016.
[21] Shlens, J, *A tutorial on principal component analysis* Systems Neurobiology Laboratory, University of California at San Diego, 2005.
[22] Bo-Suk Yang, Tian Han, and Zhong-Jun Yin, "Fault diagnosis system of induction motors using feature extraction, feature selection and classification algorithm," *JSME International Journal Series C,* vol. 49, no. 3, pp. 734-741, 2006.
[23] Laurens van der Maaten, Geoffrey Hinton, "Visualizing data using t-SNE," *J. Mach. Learn. Res.,* vol. 9, pp. 2579-2605, Nov. 2008.
[24] Hsu, C.W., and Lin, C.J, "A comparison of methods for multi-class support vector machines," *IEEE Trans. Neural Networks,* vol. 13, no. 2, pp. 415-425, 2002.

**Young-Woo Youn** received B.S. and M.S. degrees in Communication Engineering from Information and Communication University, Daejeon, Korea, in 2005 and 2007, respectively. He is currently a researcher at power apparatus research center at Korea Electrotechnology Research Institute (KERI), Changwon, Korea. His research interests are in condition monitoring and signal processing.

**Don-Ha Hwang** received B.S., M.S., and Ph.D. degrees in Electrical Engineering from Yeungnam University in 1991, 1993, and 2003, respectively. He is currently a principal researcher at Korea Electrotechnology Research Institute (KERI), Changwon, Korea. His main research interest are design, analysis, monitoring, and diagnosis of electric machines.

**Sungju Song** received his BS degree from the Department of Electronics Engineering, Myongji University, Yongin, Rep. of Korea in 2015. He is currently pursuing his MS degree at Myongji University. His current research interests include digital signal processing, motor drives and diagnosis, and partial discharge diagnosis.

**Yong-Hwa Kim** received his BS degree in electrical engineering and his PhD in electrical engineering and computer science from Seoul National University, Seoul, Rep. of Korea in 2001, and 2007, respectively. From 2007 to 2011, he was a senior researcher with the Korea Electrotechnology Research Institute, Ansan, Rep. of Korea. From 2011 to 2013, he was an assistant professor with the Division of Maritime Electronic and Communication Engineering, Mokpo National Maritime University, Mokpo, Rep. of Korea. Since 2013, he has been a faculty member with the Department of Electronic Engineering, Myongji University, where he is now an associate professor. His research interests include communication systems, digital signal processing, motor drives and diagnosis, and machine learning for smart grids.